journal of the mechanical behavior of biomedical materials 136 (2022) 105507

Contents lists available at ScienceDirect

Journal of the Mechanical Behavior of Biomedical Materials

journal homepage: www.elsevier.com/locate/jmbbm

Drivers of initial stability in cementless TKA: Isolating effects of tibiofemoral conformity and fixation features

Huizhou Yang **, Yashar Behnam, Chadd Clary, Paul J. Rullkoetter *

Center for Orthopaedic Biomechanics, University of Denver, Denver, CO, 80208, USA

ARTICLE INFO

Keywords:
Implant stability
Cementless
Tibiofemoral conformity
Fixation designs
Finite element analysis

ABSTRACT

The initial fixation of cementless tibial trays after total knee arthroplasty is critical to ensure bony ingrowth and long-term fixation. Various fixed-bearing implant designs that utilize different fixation features, surface coatings, and bony preparations to facilitate this initial stability are currently used clinically. However, the role of tibiofemoral conformity and the effect of different tray fixation features on initial stability are still unclear. This study assessed the implant stability of two TKA designs during a series of simulated daily activities including experimental testing and corresponding computational models. Tray-bone interface micromotions and the porous area ideal for bone ingrowth were investigated computationally and compared between the two designs. The isolated effect of femoral-insert conformity and fixation features on the micromotion was examined separately by virtually exchanging design features. The peak interface micromotions predicted were at least 47% different for the two designs, which was a combined result of different femoral-insert conformity (contributed 79% of the micromotion difference) and fixation features (21%). A more posterior femoral-insert contact due to lower tibiofemoral conformity in a force-controlled simulation significantly increased the micromotion and reduced the surface area ideal for bone ingrowth. The maximum difference in peak micromotions caused by only changing the fixation features was up to 33%. Overall, the moment arm from the insert articular contact point to the anterolateral tray perimeter was the primary factor correlated to peak and average micromotion. Our results indicated that tray-bone micromotion could be minimized by centralizing the load transfer and optimizing the fixation features.

1. Introduction

Total knee arthroplasty (TKA) provides reliable outcomes for patients suffering from osteoarthritis (Ritter et al., 1995). Cementless implants were developed to potentially preserve native bone stock and improve implant longevity (Dalury, 2016; Meneghini and Hanssen, 2008). Although the early designs presented a high failure rate due to aseptic loosening, newer generation cementless TKA implants, which consist of bioactive surface coatings that allow for bony ingrowth, have shown excellent outcomes comparable to the cemented TKA (Harwin et al., 2017; Nam et al., 2017). The initial fixation of the cementless tibial tray to the host bone is critical to bony ingrowth onto the porous surface of the implant. To achieve bone ingrowth, interface micromotions should ideally be less than 50 μm (Grewal et al., 1992; Ryd et al., 1995), whereas fibrous tissue would potentially develop instead when micromotions exceed 150 μm (Pilliar et al., 1986). Fixed-bearing knee prostheses are by far the most common type of total knee replacement (Kurtz, 2009). Various fixed-bearing tibial designs are currently marketed that utilize different articulations, surface coatings, fixation features, and bony preparations to facilitate the initial fixation. However, the role of implant design features, such as articular conformity and dwell position, stems, keels, and pegs, on the initial cementless fixation is not well understood.

In vitro experiments have been performed to evaluate the fixation performance for different implant fixation features by comparing the tray-bone relative displacement measured at several distinct locations around the tray-bone interface (Alipit et al., 2021; Bhimji and Meneghini, 2012; Kraemer et al., 1995; Meneghini et al., 2011; Yoshii et al., 1992; Small et al., 2019). However, these relative displacements may not represent the actual interface micromotions, as those may occur between markers, or at interfacial locations that are occluded. (Yang et al., 2020). Finite element methods have also been commonly used to

* Corresponding author. Center for Orthopaedic Biomechanics University of Denver, Room 427 2155 E. Wesley Ave. Denver, CO, 80208, USA.
** Corresponding author. Center for Orthopaedic Biomechanics University of Denver, Room 434 2155 E. Wesley Ave. Denver, CO, 80208, USA.
E-mail addresses: huizhou.yang@du.edu (H. Yang), paul.rullkoetter@du.edu (P.J. Rullkoetter).

https://doi.org/10.1016/j.jmbbm.2022.105507
Received 21 June 2022; Received in revised form 18 September 2022; Accepted 1 October 2022
Available online 5 October 2022
1751-6161/

investigate the tray-bone interface micromotions that cannot be accessed experimentally, and to determine which designs and associated features influence micromotion (Chong et al., 2016; Hashemi & Shirazi-adl, 2000; Taylor et al., 2012; Tissakht et al., 1995). Tissakht et al. (1995) assessed the immediate post-operative fixation for three fixation types (close-fit, press-fit, and screw fixation) and found that the screw fixation resulted in the lowest micromotion. The same finding was reported in another study which compared the interface micromotions between fixations with inclined porous-coated pegs and screws (Hashemi & Shirazi-adl, 2000). However, only simple axial loads were tested in these studies, whereas Bhimji and Meneghini (2012) found that physiological loading can generate larger micromotion and better detect differences between devices than simplified loading. Chong et al. (2016) utilized a validated tibial model to investigate micromotion for three implant designs under peak physiological loading conditions and found the tibial component with a mini keel showed better fixation than standard stem design. Taylor et al. (2012) have reported, however, that peak micromotions did not necessarily occur at the peak loads, highlighting the need to examine whole activity cycles.

To our knowledge, no study has investigated the effect of design on implant stability under a variety of activities of daily living with a validated computational model. Previous studies evaluated and compared the fixation performance between different implant designs under the same boundary conditions (Chong et al., 2016; Taylor et al., 2012). The impact of the conformity in the tibiofemoral articulation (which results in different tibiofemoral kinematics) was not considered. Also, the loading was typically directly applied to the tray or the insert at specific points in those studies, without considering the physiological femoral-insert contact and load transfer.

Hence, the objective of this study was to assess tray-bone interface shear and normal micromotion of two TKA designs during a series of daily activities, with the consideration of design-individual kinematics. Four previously-validated deformable tibial models were used with load and boundary conditions to replicate an experimental test series. The predicted tray-bone relative displacements were verified through comparison to experimental measurements with the same implant designs. The tray-bone interface micromotions and the porous area ideal for bone ingrowth were further investigated computationally and compared. The isolated effect of femoral-insert conformity and fixation features on the micromotion was examined separately by virtually exchanging implant design features (cone/keel, pegs, or both). It was hypothesized that a higher tibiofemoral conformity would generate less tray-bone micromotion due to the more centralized loading.

2. Methods

2.1. Experimental testing

2.1.1. Implant configurations

Two fixed-bearing and cruciate-retaining cementless knee systems were evaluated in this study. The Design I fixed-bearing tibial base has an intermediate-length cruciform stem with stepped proximal porous coating and four peripheral cylindrical pegs with a scalloped feature to ease implantation (Fig. 1a). The Design II tibial tray includes a large central keel and four bullet cruciform pegs (Fig. 1a). The underside of the tray is a porous metallic matrix. Note that Design II is commercially available and has good clinical results with respect to fixation (Harwin et al., 2017; Restrepo et al., 2020; Tarazi et al., 2020), while Design I is in pre-clinical development. Both designs were evaluated with their respective cruciate-retaining tibial insert and femoral component. The Design I knee system contains a more conforming tibiofemoral articular surface than Design II (Fig. 1b). The Design I higher conformity is hypothesized to improve fixation by providing better control of condylar translation and centralizing the contact on the tibia.

2.1.2. Mechanical testing

Six cadaveric specimens (Five males and one female, Caucasian; Age: 74.8 ± 12.8 years; Height: 172.0 ± 4.8 cm; Weight: 68.6 ± 12.5 kg) were implanted with a Design I tibial tray on one side and an equivalent size Design II tibial tray on the contralateral side by an experienced orthopaedic surgeon (total of 12 knees). The implanted tibiae were extracted from the specimen and cemented into fixtures. Target marker couples were placed at the anterior surface of the tray and rim of the tibial cortex (Fig. 2a). Each implant construct, including the implanted tibial base and bone, the articulating insert, and the femoral component, were mounted into the AMTI VIVO simulator to simulate gait (GT), deep knee bending (DKB, also referred to as 'squat' in ASTM standard), and stair descent (SD) activities (Fig. 2a). Experimental boundary conditions were derived from telemetric implant data and ASTM F3141-15 standard. The flexion/extension rotation degree of freedom (DoF) were kinematically driven while medial/lateral (ML), anterior/posterior (AP), superior/inferior (SI), varus/valgus (VV), and internal/external (IE) DoFs were load controlled. Prior to loading, arrays of infrared emitting diodes were mounted to the tibia and femoral fixturing and the location of the implanted components were digitized using an infrared stylus (Optotrack Certus, NDI, Ontario, Canada) (accuracy of 0.1 mm from the manufacturer). The three-dimensional locations of these arrays

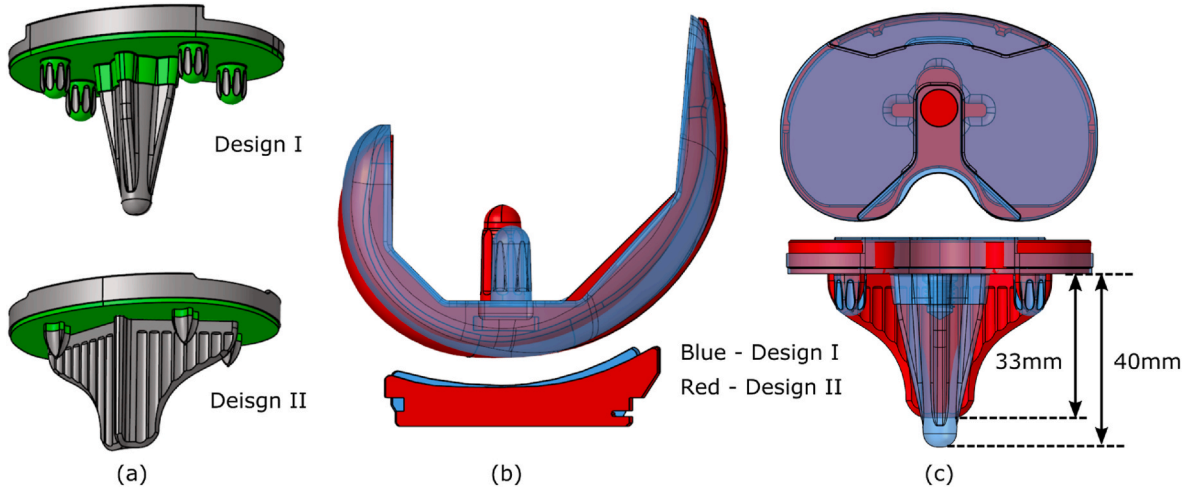

Fig. 1. (a) Geometries of the Design I and II tibial trays (porous coating surface was indicated as green color). (b) The corresponding femoral-insert articular surfaces of the two designs (Blue – Design I; Red – Design II). (c) The alignment of equivalent sizes of the Design I (size 5) and Design II (size 4) tibial bases in computational models. The Design I stem was 7 mm longer than the Design II keel.

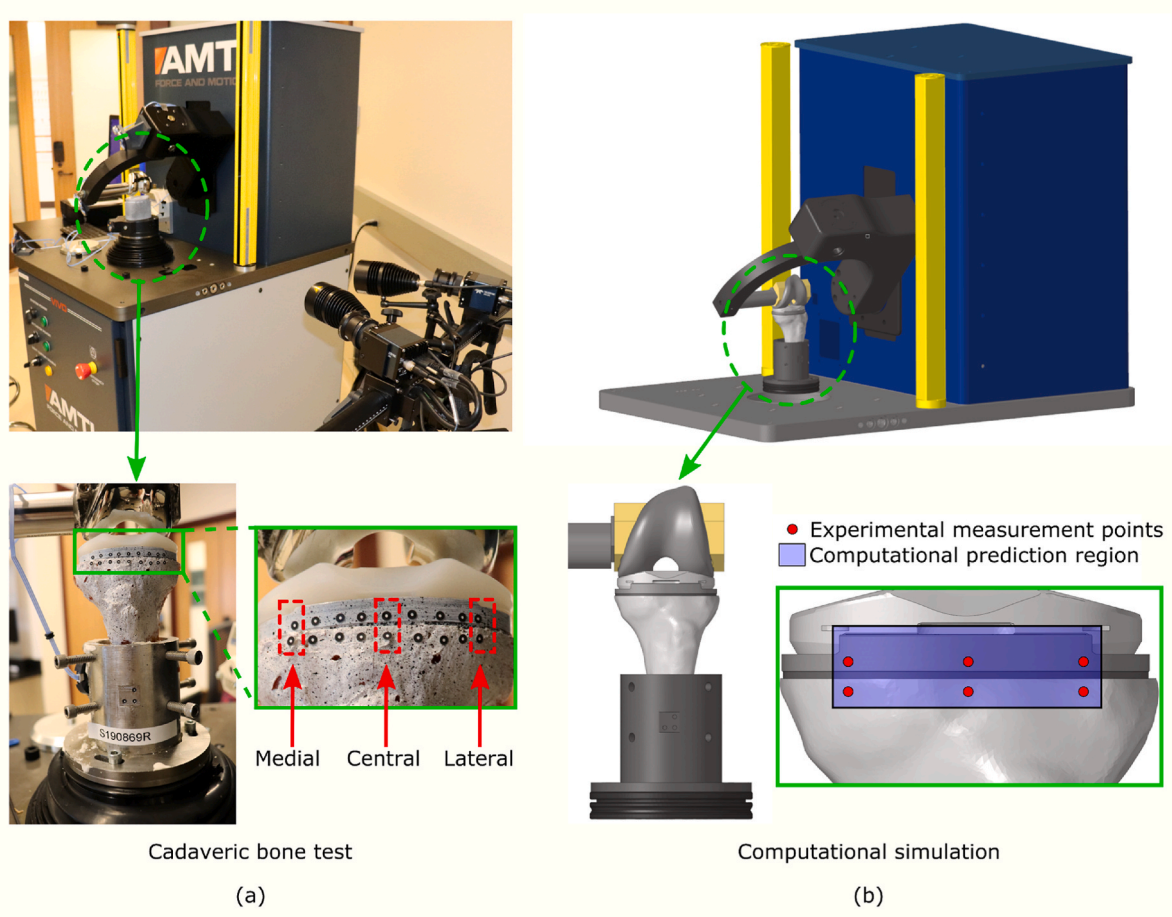

Fig. 2. (a) Experimental set up with one of the cadaveric specimens. Highlighted three marker couples (medial, central, and lateral) were used to measure the tray-bone relative displacements. (b) Computational representation using one of the validated cadaveric tibia models. Full field tray-bone relative displacements across the shaded region were predicted, which covered the measured locations.

were tracked through the loading activities, capturing the relative position of the femur on the tibia. The transformations between the two bodies were resolved using a Grood and Suntay kinematic description (Grood and Suntay, 1983). To ensure consistent application of loading cycles and an overall duty cycle for the construct, 50 cycles of each activity were performed after bedding-in under cyclic compression at a rate of 0.33Hz. Relative displacements between marker couples were recorded with the ARAMIS DIC system (GOM GmbH, Braunschweig, DE) (ISO 9513's 0.5 class of accuracy from manufacturer) for the last ten cycles.

2.2. Computational modeling

2.2.1. Baseline model set-up

Four previously validated deformable tibial models (Yang et al., 2020, 2021) (All Caucasian females; Age: 62.3 ± 11.4 years; Height: 158.2 ± 1.3 cm; Weight: 66.0 ± 22.7 kg) and best-fitting mid-size (size 5) Design I tibial tray were utilized with loading and boundary conditions to replicate the experimental testing, using ABAQUS/Standard (SIMULIA, Providence, RI). Equivalent sizes of the Design I (size 5) and Design II (size 4) knee systems were virtually implanted into the tibia models with a perfect overlap of the trays (Fig. 1c). The femoral component was meshed with rigid surface elements. The deformable TKA components and tibial bones were meshed with first-order tetrahedral elements and modeled with different material properties (Table 1). The mesh sizes and the number of materials to characterize tibial properties were identified from convergence studies in our previous work (Yang et al., 2020) and were also adopted here (Table 1). The interaction between the tibia and the porous coating was modeled with a 1.0 friction coefficient based on test data from the manufacturers. The contact between the polyethylene and metal components (insert-tray and insert-femoral) was modeled with a 0.04 friction coefficient (Godest et al., 2002). The porous and solid portions of the tray were tied together. For comparative purposes, the effect of interference fit was assessed over a range of press-fit (10, 25, 50, and 100 μm) for both designs.

Table 1
Material properties used in the computational models. Approximately 400 material properties were used for modeling the tibiae (1 material property per 4 mg/cm^3 bone apparent density).

Components	Density (g/cm^3)	Elastic moduli (MPa)	Poisson's ratios	Mesh density
Femoral - Rigid	–	–	–	1 mm
Insert - UHMWPE	0.94	571.6	0.45	1 mm
Tray solid - Titanium	4.50	110,000	0.31	1 mm
Tray porous - Titanium	1.50	2200	0.083	0.75 mm
Cortical bone	≥1	≤9922.6	0.3	0.75 mm at interface, 1.5 mm on the surface
Trabecular bone	≤1	≥79.6	0.3	0.75 mm at interface, 1.5 mm on the surface

The deformable implant-bone constructs were virtually mounted into the VIVO simulator model (Fitzpatrick et al., 2016) and loaded via the respective femoral components to simulate GT, DKB, and SD activities (Fig. 2b). The femoral-actuator and the initial femoral-insert relative positions at the beginning of each activity cycle were reconstructed by registering measured point clouds (experimentally collected by the Optotrack system prior to loading) to respective geometry files. For this, the iterative closest point algorithm was used, and the root-mean-square error of the registration was less than 0.5 mm. The VIVO output kinematics/loading conditions (FE kinematically-driven; IE, SI, ML, and VV force controlled; same as in experiments) averaged across the tested specimens were applied to the models. To exactly reproduce design-individual femoral-insert AP translations of the two designs, the AP DoF of the models was kinematically driven using the experimental AP kinematics averaged from all the tested specimens implanted with a size-5 Design I or size-4 Design II tray, respectively, for each activity. Two cycles of each activity were simulated to reach a steady state (identified from a convergence study), and the subsequent computational results were extracted from the second simulated cycle. The computational time ranged from 10–12 h for each simulation (using 10/32 processors, Intel Xeon Gold 6134 CPU @3.20Hz, 8 CPU cores).

The tray-bone relative displacement of an anterior region covering the experimental marker positions was investigated computationally (Fig. 2b). Surface node pairs at the anterior surface of the tray and bone within the region were defined as the marker couples for predicting the tray-bone displacements. The predicted marker relative displacements were then compared with experimental measurements. In order to evaluate the potential impact of variation in material properties, the elastic properties of the four tibia models were calculated using both an upper- and lower-bound elastic-density relationship (Anderson et al., 1992; Rho et al., 1995), respectively. For understanding the difference, bone apparent density ranging from 0.1–1.7 g/cm^3 corresponded to 371.8 MPã16.9 GPa and 53.9 MPã10.0 GPa when using the upper- and lower-bound elastic-density relationship respectively.

2.2.2. Model with virtually exchanged design features

In order to compare and evaluate the fixation performance of different design features, the bottom fixation features of the Design I and II tibial trays were virtually exchanged (HyperMesh, Altair Engineering Inc., Troy, Michigan) (Fig. 3), where the respective insert, insert locking mechanism, and the tibial base shape maintained unchanged. Additional tray models were created by selectively exchanging one fixation feature (pegs or the stem/keel) from the other design to investigate the effect of each fixation feature on the tray-bone interface micromotion. For example, Design I cruciform stem with Design II cruciform pegs using Design I tibial base; Design II keel with Design I cylindrical pegs using Design II tibial base. A total of eight configurations (including the two initial configurations) were evaluated (Fig. 3).

The virtual design configurations were incorporated into the baseline models and tested under the corresponding boundary conditions. When Design I or II articulations were used, the corresponding AP kinematics were applied. For example, the Design I tray using Design II pegs was tested under the Design I kinematics/loading conditions with the use of Design I insert and femoral components (the underlining indicated as 'Design I tibiofemoral conformity' subsequently); The Design II tray using the Design I stem was tested under the Design II kinematics/loading conditions with the use of Design II insert and femoral components (indicated as 'Design II tibiofemoral conformity'). For computational efficiency, the original material properties of the validated tibia models were used for these tests without including variation in material properties.

2.3. Data analysis

2.3.1. Marker relative displacements

For each activity of the experimentally tested specimens, the DIC images were post-processed to extract the relative distance of the lateral, central, and medial marker couples. The minimum distances between the marker couples were subtracted from the maximum distances over the activity cycle. This difference was averaged across all specimens with the same implant construct to determine a composite average tray-bone relative displacement. Considering the bone variations (bone anatomy and properties) between specimens and the two designs were implanted separately into the tibiae from the same specimen, a paired T-test was performed using Minitab (Minitab, LLC, State College, PA) to determine whether the means from these two groups differ. The hypotheses (H_0: $\mu_{difference} = 0$ vs. H_a: $\mu_{difference} \neq 0$) were tested at the 0.05 significance level. The percentage cycle where the maximum distance was observed was indicated on the plot showing the SI-loading & femoral AP low-points. The femoral AP low-point kinematics were calculated by averaging the medial and lateral lowest femoral points relative to the tibial insert through the activity cycle, and then averaged from all the tested specimens implanted with a size-5 Design I or size-4 Design II tray, respectively.

The same algorithm was used in computational simulations. For each activity, the relative displacement between the pre-selected node pairs

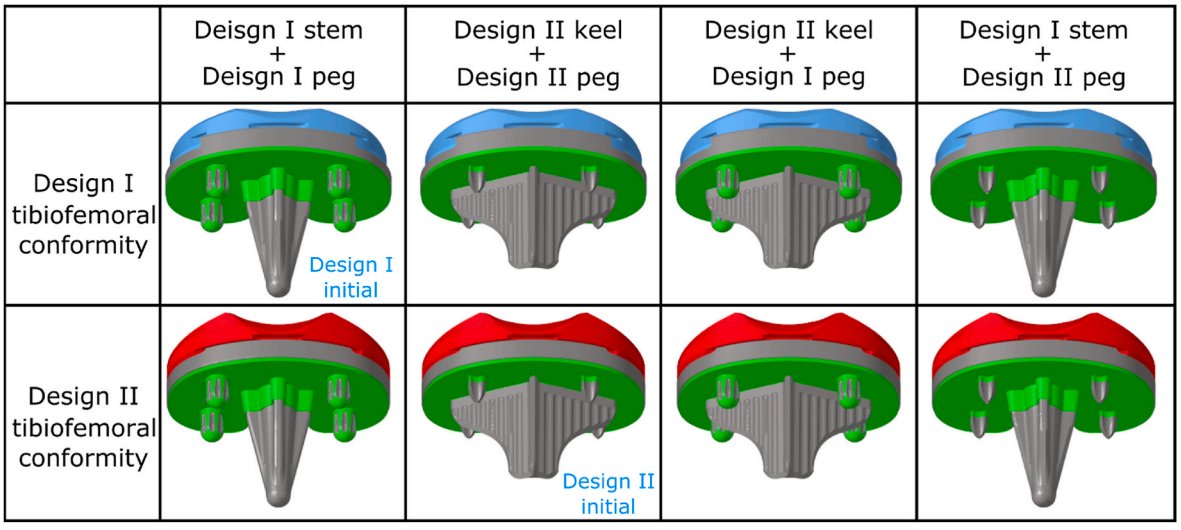

Fig. 3. Eight fixation configurations (two type of stems, pegs, and femoral-insert articular conformity). The porous coating surface was indicated as green. The initial Design I and II configurations were indicated in the figure.

was averaged across the same tibia models using the upper- and lower-bound material properties to determine the composite average tray-bone relative displacement. The computational predictions were then compared with the experimental measurements.

2.3.2. Tray-bone interface micromotions

In this study, we defined the tray-bone interface micromotion as the relative motions between the tray and the tibia contact surface. In the computational models, the changes in the distance (considering both shear and normal components) between the nodes at the tray bottom surface and the nearest node on the tibia implantation surface were used to represent the tray-bone interface micromotion. For each activity of the specimens, the micromotion at the tray-bone interface was predicted for each model configuration. The full-field micromotion contour map for the frame having the peak micromotion was also presented. The maximum value of the interface micromotions through the entire activity cycle was compared to study the effect of tibiofemoral conformity and fixation design features on the interface micromotion. Additionally, the liftoff and shear components of the interface micromotion were also compared for a more comprehensive investigation.

2.3.3. Surface area ideal for bone ingrowth

Micromotion less than 50 μm was reported as ideal for bone ingrowth (Grewal et al., 1992; Ryd et al., 1995). However, micromotion exceeding

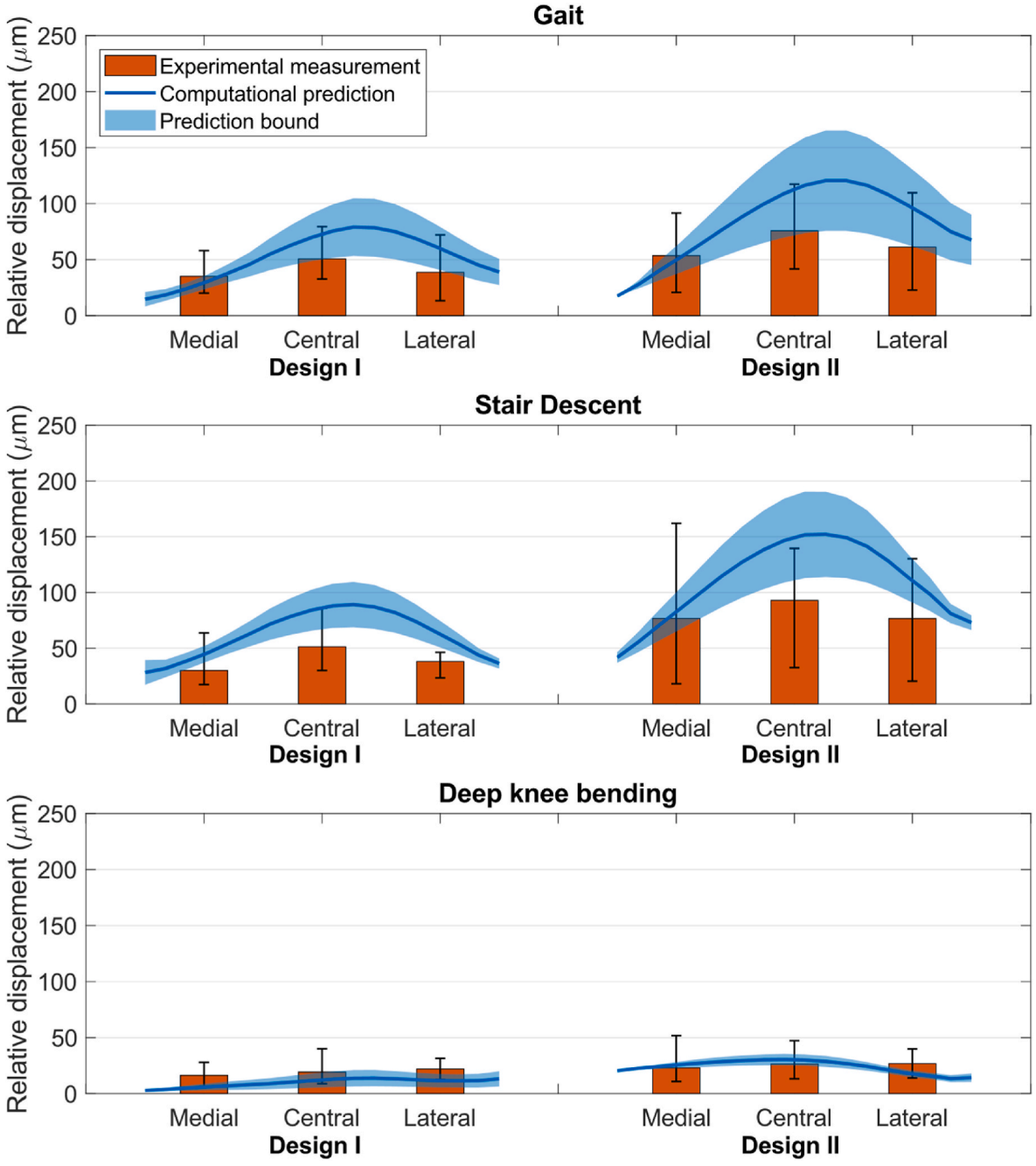

Fig. 4. Comparison between measured marker relative displacements at three locations (medial, central, and lateral) and the predictions from the computational models (averaged from the four simulated specimens) at the pre-defined anterior tray-bone surface. The prediction bounds (shaded areas) were generated by perturbing the tibial material properties within reported ranges. Error bars indicated the range of experimental measurements from all twelve physically-tested specimens.

150 μm may inhibit bone formation (Engh et al., 1992; Pilliar et al., 1986). In this study, the porous surface area experiencing micromotion less than 50 μm (indicated as SA<50 μm) was calculated as another indicator for assessing the cementless fixation. The percentage of the surface area experiencing micromotions <50 μm and >150 μm (indicated as SA%<50 μm and SA%>150 μm subsequently) was also calculated. These data were compared between the simulated models.

2.3.4. Data analysis summary

Marker relative displacements were firstly measured from experimental tests. The predicted marker displacements were then compared with those measurements to verify the computational models. For each design, the femoral low-point kinematics and femoral-insert contact position at the frame having the peak marker displacement were investigated.

After validation, the tray-bone interface micromotion and the surface area ideal for bone ingrowth were investigated computationally to evaluate the fixation performance of different implant designs. The isolated impact of articulation conformity and fixation design features were studied and discussed respectively. The outcomes in the next Results section were presented in the same order.

3. Results

3.1. Experimental measurements

The maximum marker relative displacements for the Design II knee system (mean ± SD: 104.5 ± 47.3 μm) were consistently higher compared with Design I (56.4 ± 18.7 μm). A statistically significant difference was found between the two groups ($P = 0.022$), with a (−86.0 ~ −10.3 μm) 95% confidence interval for the difference in the marker relative displacements between Design I and Design II.

For Design II, the tray-bone relative displacements were the highest in stair descent activity, followed by gait, and were much smaller in deep knee bending activity. For Design I, the tray-bone relative displacements were very similar in gait and stair descent. For the activities generating higher tray-bone relative displacements (gait and stair descent), the central regions consistently had the maximum displacements (Fig. 4).

3.2. Comparison of measured and predicted marker relative displacements

Higher maximum marker relative displacements were also predicted for the Design II group (158.2 ± 22.7 μm) compared with the Design I group (93.2 ± 17.1 μm). The difference was statistically significant at $\alpha = 0.05$ level ($P = 0.003$), with a (−87.9 ~ −42.1 μm) (Design I vs. Design II) 95% confident interval. The computational predictions correctly represented the experimental trends (the order of maker displacement between the two designs, for each design among the three activities, and for each activity among the three marker locations) and were within the measurements in magnitude (Fig. 4).

The maximum marker relative displacement occurred at the same percent cycle both experimentally and computationally (Fig. 5). The peak tray-bone relative displacement occurred at (17%, 25%, 21%) (GT, SD, DKB) and (17%, 31%, 21%) of the activity cycle for Design I and II, respectively. For gait and stair descent activities, the peak marker displacements did not occur at the frames having the maximum axial loads but were associated with the femoral-insert posterior translation (Fig. 5-left). The corresponding femoral-insert contact locations of the Design II knee system were on average of 2.5 and 4.0 mm more posterior than Design I for gait and stair descent activities, respectively (Fig. 5-right).

Note: The marker relative displacement was the only parameter that was both experimentally measured and computationally predicted in this study. The results below this point were all investigated computationally.

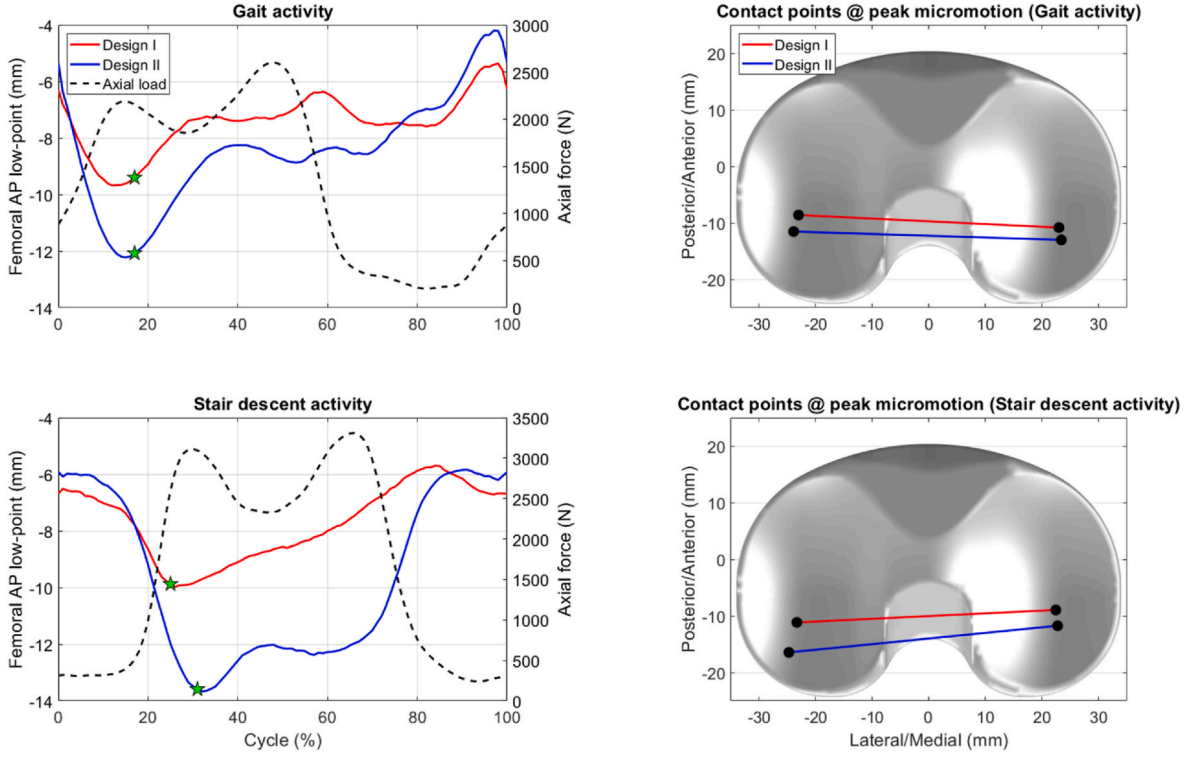

Fig. 5. (Left) The AP movement of the lowest femoral points and the axial forces during gait and stair descent activities for the two designs. The percentage cycles where the peak marker relative displacement occurred were marked out. (Right) The femoral-insert contact locations at the frame having peak marker relative displacement. *Note: The Peak marker relative displacement and interface micromotion occurred at the same frame.*

3.3. Tray-bone interface micromotion

The peak tray-bone interface micromotion predicted for the Design II knee system was on average at least 47% larger than those predicted for Design I (Fig. 6). The liftoff and shear components of the micromotion had the same trend as the total micromotion (Fig. 6). For better visualization of the resulting micromotion variations and distributions, the full-field interface micromotion contour maps are presented for the first specimen during stair descent activity (the activity had the highest micromotions), which covered all the fixation configurations (Fig. 7).

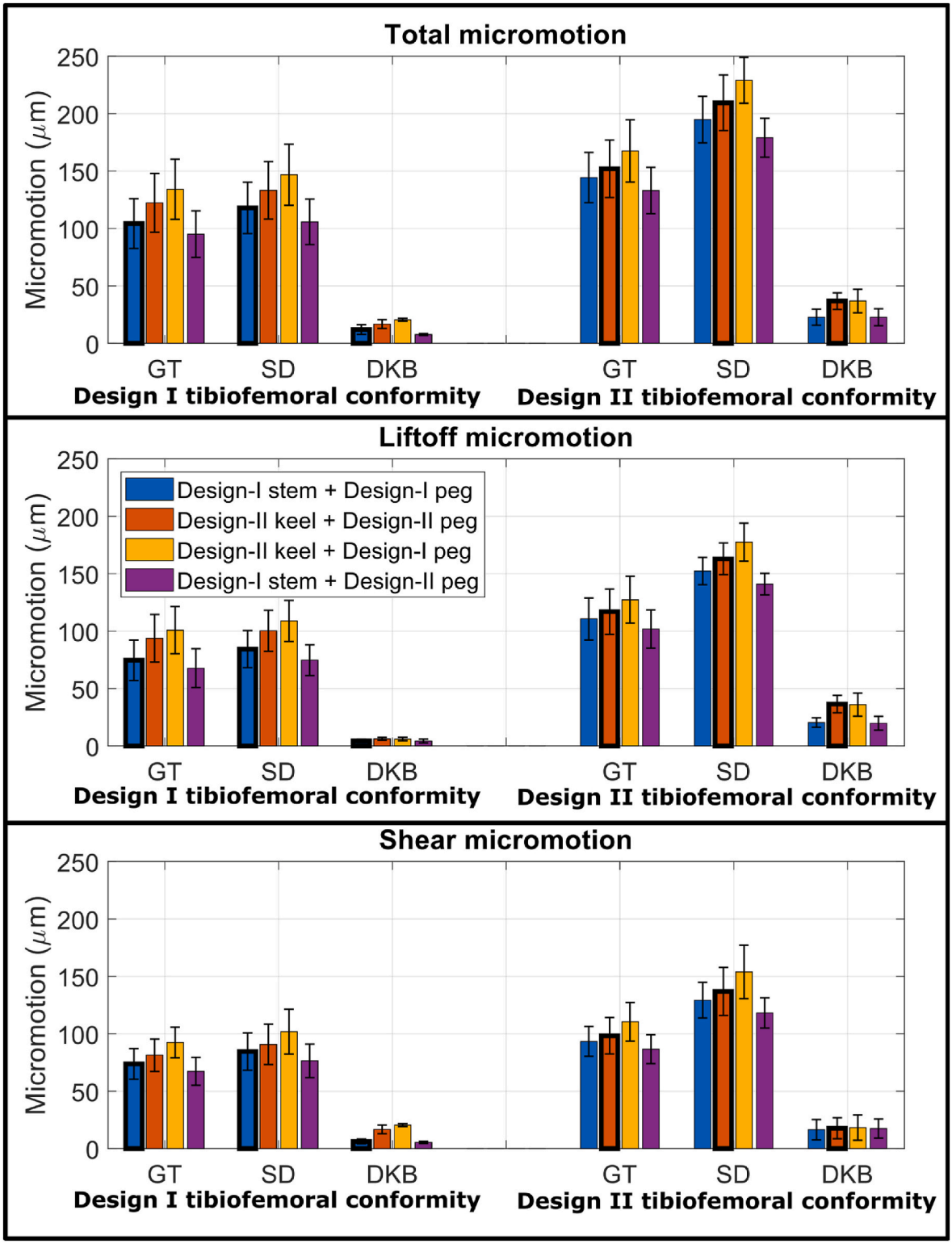

Fig. 6. Predicted peak interface micromotion (mean ± SD) for each fixation configuration during all activities. Data of the initial Design I and II models were indicated in bars with bold edge. (The micromotion differences between Design I and II were calculated by comparing the bold edged blue bars versus bold edged red bars in different categories).

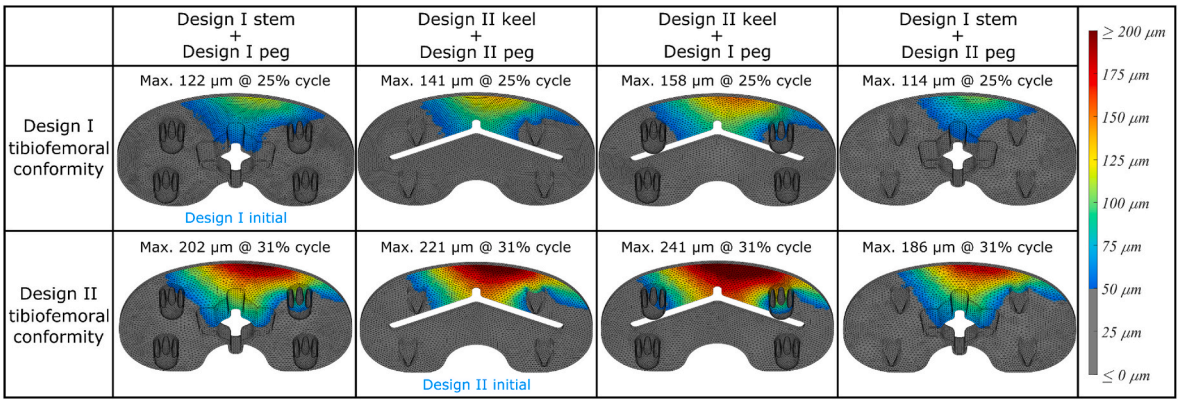

Fig. 7. The predicted full-field interface micromotion contour maps at the frames having peak micromotion for each fixation configuration. (The presented plots were from the first specimen during stair descent activity, which had the maximum micromotion in this study).

3.3.1. *Effect of articulation conformity on micromotion*

The peak micromotion changes caused purely by the conformity difference were on average 34.8, 76.6, and 15.4 μm (GT, SD, DKB), which accounts for 73%, 84%, and 62% of the total micromotion differences during the three activities, with the greater tibiofemoral conformity showing the better fixation performance (Fig. 6).

3.3.2. *Effect of fixation features on micromotion*

The peak micromotion changes caused purely by the design feature difference were on average 12.8, 14.9, 9.5 μm (GT, SD, DKB), which accounts for the remaining 27%, 16%, and 38% of the total micromotion differences, with the Design I fixation features having the better fixation performance.

For all fixation configurations, the pattern using Design I cruciform stem with Design II cruciform pegs always resulted in the lowest peak interface micromotions (indicated as the 'lower micromotion configuration'), whereas its opposite configuration, Design II keel with Design I cylindrical pegs, consistently had the highest micromotions (indicated as the 'higher micromotion configuration') (Figs. 6 and 7). The peak micromotions predicted for the 'higher micromotion configuration' were on average of 36.8 (34%), 46.1 (34%), and 13.5 μm (116%) larger than those predictions for the 'lower micromotion configuration' under the same conditions during GT, SD, and DKB activities, respectively.

3.4. *Surface area ideal for bone ingrowth*

The SA%<50 μm and SA%>150 μm were investigated and compared (Fig. 8). The predicted SA%<50 μm for Design I ranged from 78% to 92% for the two activities generating the highest micromotion (GT and SD), without any SA%>150 μm. In comparison, Design II generated lower values for SA%<50 μm, ranging from 71% to 81%, and higher values for SA%>150 μm, ranging from 0% to 10%. Both designs achieved 100% SA%<50 μm during deep knee bending activity. The 'lower micromotion configuration' was predicted to consistently have the highest SA%<50 μm for gait and stair descent activities, ranging from 81% to 95% using Design I articulation and from 72% to 85% using Design II articulation. In comparison, the 'higher micromotion configuration' generated the highest SA%>150 μm, ranging from 0% to 3% using Design I articulation and up to 14% using Design II articulation.

The SA<50 μm was investigated to assess the potential for osseointegration (Fig. 9). The predicted SA<50 μm for Design I was on average 9.9 (53%), 9.7 (56%), and 8.7 cm^2 (37%) larger than Design II during GT, SD, and DKB activities, respectively. Among all the fixation configurations, the initial configuration of Design I consistently had the highest SA<50 μm, although the 'lower micromotion configuration' had the highest SA%<50 μm. This was because Design I had a larger initial porous area. Similarly, the initial configuration of Design II consistently had the lowest SA<50 μm, even though the 'worst configuration' had the lowest SA%<50 μm.

The initial porous coating areas for the equivalent sizes of the Design I (size 5) and II (size 4) were 32.3 and 23.7 cm^2, respectively. Design I had 37% more porous area than Design II, with 2.4 cm^2 more at pegs, 5.0 cm^2 more around the stem, and 1.2 cm^2 more on the baseplate (Fig. 1). The initial porous coating area of the 'lower micromotion configuration' was 29.9 or 28.7 cm^2 when using the Design I or II tray baseplate, respectively. The initial porous coating area of the '-higher micromotion configuration' was 27.3 or 26.1 cm^2.

3.5. *Effect of interference fit for tray in bone on micromotion*

The maximum interface micromotion predicted with 100 μm interference fit reduced on average by 33% compared to the line-to-line fit

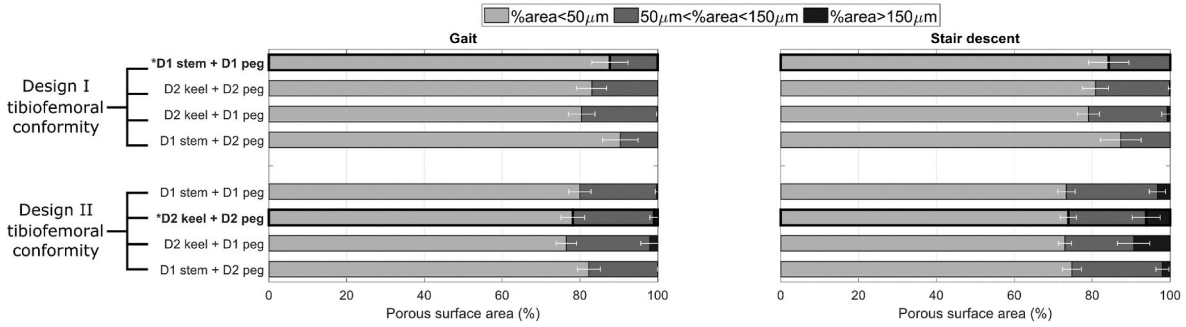

Fig. 8. The predicted proportion (mean ± SD) of porous coating surface area experiencing micromotions <50 μm and >50 μm for each fixation configuration at the frame having peak micromotions during gait and stair descent activities. Data of the initial Design I and II models were indicated with * and in bold font. (D1 – Design I; D2 – Design II) *Note: Deep knee bending activity always had 100% area experiencing micromotion less than* 50 μm, *and the data were thus not shown.*

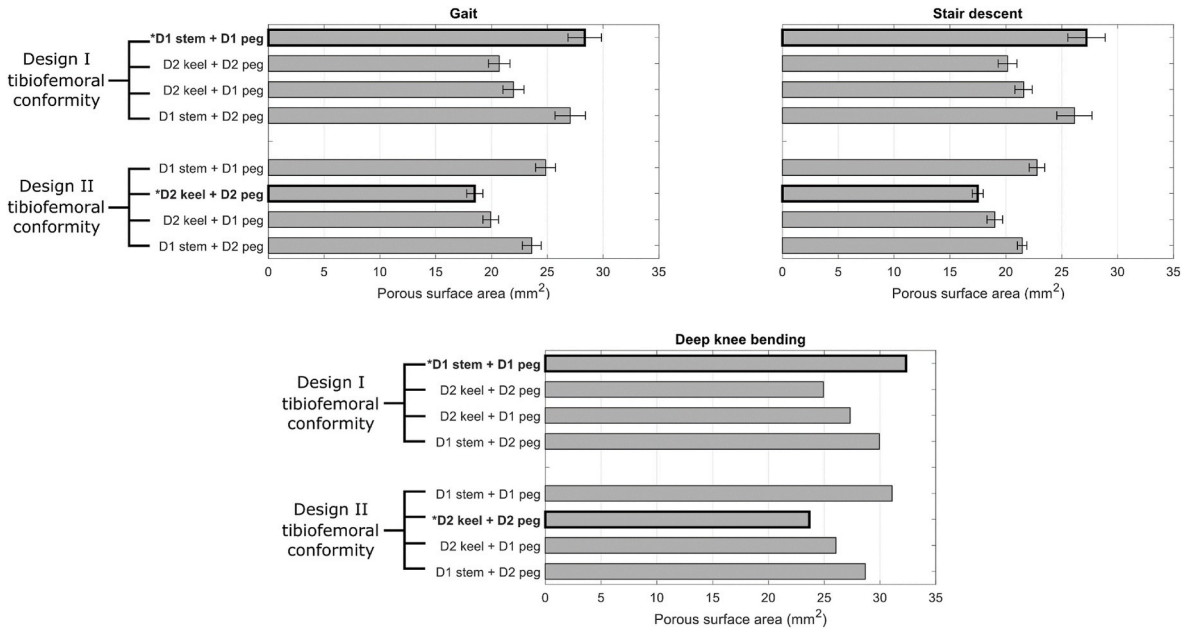

Fig. 9. The predict surface area (mm^2) (mean ± SD) favorable for bone ingrowth (<50 μm) for each fixation configuration at the frame having peak micromotions during all three activities. Data of the initial Design I and II models were indicated with * and in bold font. *Note: Deep knee bending activity always had 100% area experiencing micromotion less than* 50 μm*, and the values in the bottom plot were thus equal to the total porous surface area of each fixation configuration.*

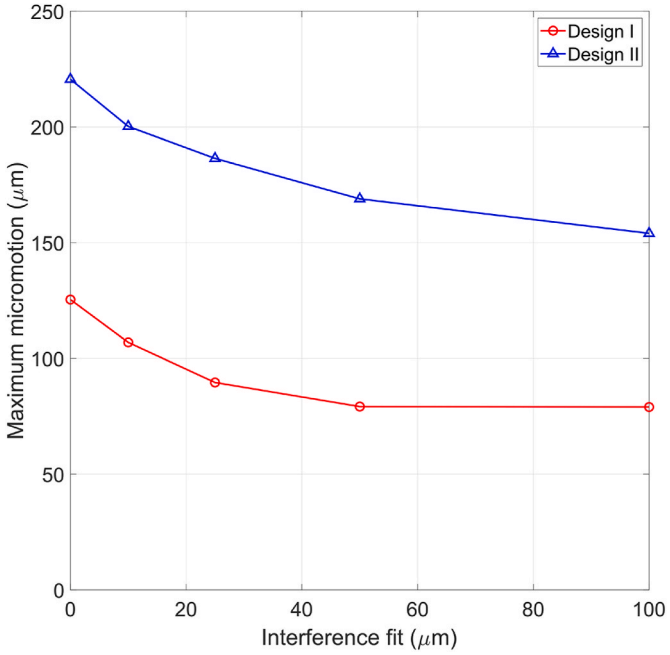

Fig. 10. The impact of interference fits on tray-bone micromotion predictions. (The presented data were from the first specimen during stair descent activity, which had the maximum micromotion in this study.

(Fig. 10). The impact of interference fits gradually decreased as the value of the interference fit increased.

4. Discussion

The initial fixation of cementless tibial trays after total knee arthroplasty is crucial to bone ingrowth onto the porous surface of the implants. This study experimentally and computationally assessed the fixation stability of two TKA designs. The tray-bone interface micromotion and the surface area ideal for bone ingrowth were investigated computationally. The effect of tibiofemoral conformity and fixation designs on the micromotion was isolated and evaluated by virtually exchanging the fixation features. In this study, the Design I and II tibial trays were implanted to the tibia model at the same location, with the outer edge profiles overlapped perfectly, which is thus the most ideal for comparison.

In this study, the tray-bone anterior surface relative motions during gait, deep knee bending, and stair descent were measured from six cadaveric tibia pairs implanted with Design I and II. Statistically significant differences ($\mu_{difference} = 48.1$ μm, $P = 0.022$) was found between two design groups, with Design II groups consistently showing larger surface displacements. The computational predictions were verified with the measured surface tray-bone relative displacements and differentiated between locations and activities. The predicted marker relative displacements accurately captured the trend and were within the range of measurements in magnitude, which improved the reliability of the outcomes from the computational simulations. The predicted peak interface micromotion consistently occurred at the anterior edge of the tibial baseplate, same as the location reported by Glenday et al. (2021) and Navacchia et al. (2018). We also found that the peak micromotion did not necessarily occur at the frame having the peak axial load but was more associated with the femoral-insert posterior translation. This result was similar to those of a previous study (Taylor et al., 2012), where it was reported that the peak micromotions for level walking occurred when there were lower axial forces but moderate varus-valgus moments. These findings highlight the need to examine the whole activity cycle to determine the implant fixation stability.

Consistently lower tray-bone relative displacements were experimentally observed for the Design I knee system comparing with Design II during all activities, which indicated a potentially better fixation performance. However, these measured marker relative displacements may not represent the actual interface micromotions. The outcome from computational simulations supported the experimental findings. It was found that the Design I knee system showed better initial fixation stability than Design II in terms of both peak micromotion and porous area favorable for bone ingrowth (SA<50 μm). The peak interface micromotions predicted for Design II were at least 47% larger than those predictions for Design I. The difference in peak micromotions was a

combined result of the different femoral-insert articulation conformities and fixation designs. For the two activities generating the highest micromotions (GT and SD), the effect of conformity contributed an average of 79% of the peak micromotion difference, and the effect of fixation features accounted for the rest 21%.

The influence of conformity on the micromotion was caused by the corresponding change in femoral-insert AP translations. The femoral-insert contact location at the frame having peak micromotions was found to be 2.5–4.0 mm more posterior for Design II than Design I during the activities generating the highest micromotions (GT and SD). The greater posterior offset of the load maximized the flexion-extension moment and anterior tray micromotions (Fig. 6). This was in line with our previous findings that a more posterior tray-bone alignment and an increased posterior load resulted in more micromotion due to the same mechanism (Yang et al., 2020, 2022). Although lower tibiofemoral conformity may lower the wear rate (Brockett et al., 2017; Luger et al., 1997), it reduces the implant stability in terms of the tray-bone interface micromotion. However, it should be noted that Design II is commercially available and has demonstrated excellent clinical outcomes in multiple studies with five-year follow-up (Harwin et al., 2017; Restrepo et al., 2020; Tarazi et al., 2020). 98.4% survivorship for aseptic loosening as the endpoint were reported in 296 Design II TKAs (Restrepo et al., 2020).

Previous studies have shown that the fixation features could have a considerable impact on the interface micromotion (Alipit et al., 2021; Bhimji and Meneghini, 2014; Chong et al., 2016; Hashemi & Shirazi-adl, 2000; Meneghini et al., 2011; Taylor et al., 2012). In this study, the predicted peak interface micromotions from models using the Design I fixation features were on average of 11% less than those predictions from models using the Design II fixation features during GT and SD activities under the same boundary conditions. For single fixation feature comparison (stem or peg), the Design I cruciform stem resulted in less micromotion than the Design II keel, while the Design II bullet cruciform pegs presented a better performance in resisting micromotion than the Design I cylindrical pegs. For the combined configurations of the studied fixation features, the maximum difference in peak micromotions between the 'lower micromotion' (Design I stem with Design II pegs) and the 'higher micromotion configuration' (Design II keel with Design I pegs) was up to 65.0 μm (33%). This finding indicated the potential to reduce cementless interface micromotion by optimizing the fixation features.

The cementless fixation relies on the bone ingrowth into the porous spaces of the tibial component. More contact area with osseointegration indicates a stronger fixation. Several studies have investigated the prosthesis area with micromotion below threshold values to assess the implant fixation (Chong et al., 2016; Glenday et al., 2021). In the current study, the porous surface area experiencing micromotion less than 50 μm (SA<50 μm) was investigated as another indicator for assessing cementless fixation stability. The predicted SA<50 μm for Design I was on average of 42% larger than Design II during GT and SD activities, which indicated much stronger fixation stability for Design I. It should be noted that although the 'lower micromotion configuration' consistently generated the lowest peak interface micromotions and had the highest SA%<50 μm, Design I still had the larger SA<50 μm than the 'lower micromotion configuration' due to the more initial porous area. Similarly, Design II always had the smallest SA<50 μm even though the 'higher micromotion configuration' generated higher micromotions than Design II. This finding was in line with a previous study (Chong et al., 2016), where it was observed that the design with larger micromotions could have a greater extent of osseointegration. Hence, solely using the peak interface micromotion (or using SA%<50 μm) may not be enough to evaluate the implant fixation performance, as the fixation strength is determined by how much bone grows into the porous surface, and these parameters (peak micromotion and SA%<50 μm) are not direct indicators. Therefore, we suggest investigating porous surface area favorable for bone ingrowth as the priority indicator to assess cementless fixation. This finding also implied the potential to improve implant stability by intentionally increasing the porous coating coverage without the need to minimize the micromotion, which might be the best solution for cementless implant designs that require enough fixation stability while maintaining low articulation conformity. However, the drawback of the excessive use of porous coating (For example, increase the difficulty for revision and increase the risk of stress shielding) were not discussed here and thus needed attention.

This study has limitations to note. Firstly, the computational analysis was based on four validated tibiae specimens. Although much better than the previous studies that use a single tibia, caution should still be taken when extrapolating our findings to a larger patient population. Secondly, the same contact parameters at the porous-bone interface were used for the two designs without considering the impact of different porous coating techniques. However, our previous study showed less than 10% difference in micromotions when perturbing the coefficient of friction from 0.6 to 1.4. Therefore, the influence of the possible difference in contact friction between the two evaluated designs was limited. Thirdly, no interference fit was assumed between the prostheses and the bone for direct comparison of features. Although the impact of interference fits was considerable (Fig. 10), the achieved interference fit is potentially lower due to the removal of further material during implantation (Abdul-Kadir et al., 2008), and the pre-stresses caused by the interference fit would reduce over time due to the viscoelasticity of bone (Norman et al., 2005). Therefore, the actual influence of interference fits on the micromotion would likely be smaller than the predicted value. Finally, the isolated effect of fixation design features on micromotion could be validated by experiments applying the same AP kinematics to different implant designs. Future studies are expected to verify our findings by doing so.

In general, this study assessed the primary stability of two cementless TKA designs during a series of daily activities, with the consideration of design-individual kinematics. The impact of tibiofemoral conformity and fixation designs were isolated by virtually exchanging the fixation features, which allowed the investigation of the isolated effect of these two factors. The tibiofemoral conformity had the most significant impact on the tray-bone interface micromotion. A more posterior femoral-insert contact due to lower conformity significantly increased the micromotion and reduced the surface area ideal for bone ingrowth. The impact of different fixation designs was relatively smaller but still considerable, indicating the potential to improve implant stability by optimizing the fixation designs. However, cautions should be taken for the corresponding changes in the porous coating area when changing fixation designs. Solely using the peak interface micromotion was not enough to evaluate the fixation performance as the design with larger micromotions could have a greater extent of osseointegration. The workflow presented in this study could be used as a benchmark for assessing future implant designs.

CRediT authorship contribution statement

Huizhou Yang: Writing – review & editing, Writing – original draft, Methodology, Investigation, Formal analysis, Conceptualization. **Yashar Behnam:** Writing – review & editing, Methodology, Investigation, Formal analysis, Data curation. **Chadd Clary:** Writing – review & editing, Resources, Project administration, Methodology, Investigation, Funding acquisition, Formal analysis, Data curation, Conceptualization. **Paul J. Rullkoetter:** Writing – review & editing, Supervision, Resources, Project administration, Methodology, Funding acquisition, Conceptualization.

Declaration of competing interest

The authors declare the following financial interests/personal relationships which may be considered as potential competing interests: Paul Rullkoetter reports financial support was provided by DePuy

Synthes.

Data availability

The authors do not have permission to share data.

Acknowledgements

This study was funded by DePuy Synthes Products, LLC.

References

Abdul-Kadir, M.R., Hansen, U., Klabunde, R., Lucas, D., Amis, A., 2008. Finite element modelling of primary hip stem stability: the effect of interference fit. J. Biomech. 41 (3), 587–594. https://doi.org/10.1016/j.jbiomech.2007.10.009.

Alipit, V., Kirk, A., Scholl, D., Schmidig, G., Springer, B.D., Lee, G.C., 2021. Micromotion analysis of various tibial constructs in moderate tibial defects in revision total knee arthroplasty. J. Arthroplasty 36 (1), 362–367. https://doi.org/10.1016/j.arth.2020.07.013 e1.

Anderson, M.J., Keyak, J.H., Skinner, H.B., 1992. Compressive mechanical properties of human cancellous bone after gamma irradiation. J. Bone Joint Surg. 74 (5), 747–752. https://doi.org/10.2106/00004623-199274050-00014.

Bhimji, S., Meneghini, R.M., 2012. Micromotion of cementless tibial baseplates under physiological loading conditions. J. Arthroplasty 27 (4), 648–654. https://doi.org/10.1016/j.arth.2011.06.010.

Bhimji, S., Meneghini, R.M., 2014. Micromotion of cementless tibial baseplates: keels with adjuvant pegs offer more stability than pegs alone. J. Arthroplasty 29 (7), 1503–1506. https://doi.org/10.1016/j.arth.2014.02.016.

Brockett, C.L., Carbone, S., Fisher, J., Jennings, L.M., 2017. Influence of conformity on the wear of total knee replacement: an experimental study. Proc. IME H J. Eng. Med. 232 (2), 127–134. https://doi.org/10.1177/0954411917746433.

Chong, D.Y.R., Hansen, U.N., Amis, A.A., 2016. Cementless mis mini-keel prosthesis reduces interface micromotion versus standard stemmed tibial components. J. Mech. Med. Biol. 16, 1650070 https://doi.org/10.1142/s0219519416500706, 05.

Dalury, D.F., 2016. Cementless total knee arthroplasty. The bone & Joint Journal 98-B, 867–873. https://doi.org/10.1302/0301-620X.98B7.37367.

Engh, C.A., O'Connor, D., Jasty, M., Mcgovern, T.F., Bobyn, J.D., Harris, W.H., 1992. Quantification of Implant Micromotion, Strain Shielding, and Bone Resorption with Porous-Coated Anatomic Medullary Locking Femoral Prostheses. In: Clinical Orthopaedics and Related Research, pp. 13–29. https://doi.org/10.1097/00003086-199212000-00005. NA;(285).

Fitzpatrick, C.K., Maag, C., Clary, C.W., Metcalfe, A., Langhorn, J., Rullkoetter, P.J., 2016. Validation of a new computational 6-DOF knee simulator during dynamic activities. J. Biomech. 49 (14), 3177–3184. https://doi.org/10.1016/j.jbiomech.2016.07.040.

Glenday, J.D., Wright, T.M., Lipman, J.D., Sculco, P.K., Mayman, D.J., Vigdorchik, J.M., Quevedo Gonzalez, F.J., 2021. Effect of varus alignment on the bone–implant interaction of a cementless tibial baseplate during gait. J. Orthop. Res. 40 (4), 816–825. https://doi.org/10.1002/jor.25129.

Grewal, R., Rimmer, M., Freeman, M., 1992. Early migration of prostheses related to long-term survivorship. Comparison of tibial components in knee replacement. The Journal of Bone and Joint Surgery. British 74-B (2), 239–242. https://doi.org/10.1302/0301-620x.74b2.1544960.

Godest, A.C., Beaugonin, M., Haug, E., Taylor, M., Gregson, P., 2002. Simulation of a knee joint replacement during a gait cycle using explicit finite element analysis. J. Biomech. 35 (2), 267–275. https://doi.org/10.1016/s0021-9290(01)00179-8.

Grood, E.S., Suntay, W.J., 1983. A joint coordinate system for the clinical description of three-dimensional motions: application to the knee. J. Biomech. Eng. 105 (2), 136–144. https://doi.org/10.1115/1.3138397.

Harwin, S.F., Patel, N.K., Chughtai, M., Khlopas, A., Ramkumar, P.N., Roche, M., Mont, M.A., 2017. Outcomes of newer generation cementless total knee arthroplasty: beaded periapatite-coated vs highly porous titanium-coated implants. J. Arthroplasty 32 (7), 2156–2160. https://doi.org/10.1016/j.arth.2017.01.044.

Hashemi, A., Shirazi-adl, A., 2000. Finite element analysis of tibial implants — effect of fixation design and friction model. Comput. Methods Biomech. Biomed. Eng. 3 (3), 183–201. https://doi.org/10.1080/10255840008915264.

Kraemer, W.J., Harrington, I.J., Hearn, T.C., 1995. Micromotion secondary to axial, torsional, and shear loads in two models of cementless tibial components. J. Arthroplasty 10 (2), 227–235. https://doi.org/10.1016/s0883-5403(05)80132-9.

Kurtz, S.M., 2009. UHMWPE Biomaterials Handbook: Ultra High Molecular Weight Polyethylene in Total Joint Replacement and Medical Devices (Plastics Design Library, second ed. Academic Press.

Luger, E., Sathasivam, S., Walker, P.S., 1997. Inherent differences in the laxity and stability between the intact knee and total knee replacements. Knee 4 (1), 7–14. https://doi.org/10.1016/s0968-0160(96)00224-4.

Meneghini, R.M., Hanssen, A.D., 2008. Cementless fixation in total knee arthroplasty: past, present, and future. J. Knee Surg. 21 (4), 307–314. https://doi.org/10.1055/s-0030-1247837.

Meneghini, R., Daluga, A., Soliman, M., 2011. Mechanical stability of cementless tibial components in normal and osteoporotic bone. J. Knee Surg. 24, 191–196. https://doi.org/10.1055/s-0031-1280879, 03.

Nam, D., Kopinski, J.E., Meyer, Z., Rames, R.D., Nunley, R.M., Barrack, R.L., 2017. Perioperative and early postoperative comparison of a modern cemented and cementless total knee arthroplasty of the same design. J. Arthroplasty 32 (7), 2151–2155. https://doi.org/10.1016/j.arth.2017.01.051.

Navacchia, A., Clary, C.W., Wilson, H.L., Behnam, Y.A., Rullkoetter, P.J., 2018. Validation of model-predicted tibial tray-synthetic bone relative motion in cementless total knee replacement during activities of daily living. J. Biomech. 77, 115–123. https://doi.org/10.1016/j.jbiomech.2018.06.024.

Norman, T.L., Ackerman, E.S., Smith, T.S., Gruen, T.A., Yates, A.J., Blaha, J.D., Kish, V. L., 2005. Cortical bone viscoelasticity and fixation strength of press-fit femoral stems: an in-vitro model. J. Biomech. Eng. 128 (1), 13–17. https://doi.org/10.1115/1.2133766.

Pilliar, R.M., Lee, J.M., Maniatopoulos, C., 1986. Observations on the Effect of Movement on Bone Ingrowth into Porous-Surfaced Implants. In: Clinical Orthopaedics and Related Research, pp. 108–113. https://doi.org/10.1097/00003086-198607000-00023. NA;(208).

Restrepo, S., Hozack, W.J., Smith, E.B., 2020. Minimum five-year follow-up of a novel 3D-printed tibial baseplate for cementless total knee arthroplasty. Orthopaedic Proceedings 102-B. No. SUPP_91.

Rho, J., Hobatho, M., Ashman, R., 1995. Relations of mechanical properties to density and CT numbers in human bone. Med. Eng. Phys. 17 (5), 347–355. https://doi.org/10.1016/1350-4533(95)97314-f.

Ritter, M.A., Albohm, M.J., Keating, E.M., Faris, P.M., Meding, J.B., 1995. Comparative outcomes of total joint arthroplasty. J. Arthroplasty 10 (6), 737–741. https://doi.org/10.1016/S0883-5403(05)80068-3.

Ryd, L., Albrektsson, B., Carlsson, L., Dansgard, F., Herberts, P., Lindstrand, A., Regner, L., Toksvig-Larsen, S., 1995. Roentgen stereophotogrammetric analysis as a predictor of mechanical loosening of knee prostheses. The Journal of Bone and Joint Surgery. British 77-B (3), 377–383. https://doi.org/10.1302/0301-620x.77b3.7744919.

Small, S.R., Rogge, R.D., Reyes, E.M., Seale, R.B., Elliott, J.B., Malinzak, R.A., 2019. Primary stability in cementless rotating platform total knee arthroplasty. J. Knee Surg. 34, 192–199. https://doi.org/10.1055/s-0039-1694055, 02.

Tarazi, J.M., Salem, H.S., Ehiorobo, J.O., Sodhi, N., Mont, M.A., Harwin, S.F., 2020. Cementless tritanium baseplate total knee arthroplasty: survivorship and outcomes at 5-year minimum follow-up. J. Knee Surg. 33 (9), 862–865. https://doi.org/10.1055/s-0040-1712983.

Taylor, M., Barrett, D.S., Deffenbaugh, D., 2012. Influence of loading and activity on the primary stability of cementless tibial trays. J. Orthop. Res. 30 (9), 1362–1368. https://doi.org/10.1002/jor.22056.

Tissakht, M., Eskandari, H., Ahmed, A., 1995. Micromotion analysis of the fixation of total knee tibial component. Comput. Struct. 56 (2–3), 365–375. https://doi.org/10.1016/0045-7949(95)00029-g.

Yang, H., Bayoglu, R., Renani, M.S., Behnam, Y., Navacchia, A., Clary, C., Rullkoetter, P. J., 2020. Validation and sensitivity of model-predicted proximal tibial displacement and tray micromotion in cementless total knee arthroplasty under physiological loading conditions. J. Mech. Behav. Biomed. Mater. 109, 103793 https://doi.org/10.1016/j.jmbbm.2020.103793.

Yang, H., Bayoglu, R., Clary, C., Rullkoetter, P.J., 2021. Impact of surgical alignment, tray material, PCL condition, and patient anatomy on tibial strains after TKA. Med. Eng. Phys. 88, 69–77. https://doi.org/10.1016/j.medengphy.2021.01.001.

Yang, H., Bayoglu, R., Clary, C., Rullkoetter, P.J., 2022. Impact of patient, surgical, and implant design factors o predicted tray-bone interface micromotions in cementless total knee arthroplasty. J. Orthop. Res. 1–15. https://doi.org/10.1002/jor.25344.

Yoshii, I., Whiteside, L.A., Milliano, M.T., White, S.E., 1992. The effect of central stem and stem length on micromovement of the tibial tray. J. Arthroplasty 7, 433–438. https://doi.org/10.1016/s0883-5403(07)80036-2.